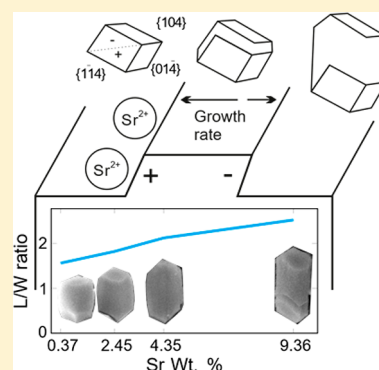


Enhanced Crystallographic Incorporation of Strontium(II) Ions into Calcite via Preferential Adsorption at Obtuse Growth Steps

David J. Hodkin,[†] Douglas I. Stewart,[‡] James T. Graham,[§] Giannantonio Cibin,^{||} and Ian T. Burke^{*,†}[†]School of Earth and Environment, University of Leeds, Leeds LS2 9JT, U.K.[‡]School of Civil Engineering, University of Leeds, Leeds LS2 9JT, U.K.[§]National Nuclear Laboratory, Sellafield, Cumbria CA20 1PG, U.K.^{||}Diamond Light Source, Harwell Science and Innovation Campus, Didcot OX11 0DE, U.K.

Supporting Information

ABSTRACT: Sr-containing calcium carbonates were precipitated from solutions containing $\text{Ca}(\text{OH})_2$, SrCl_2 , and Na_2CO_3 in a reactor where constant solution composition was maintained. The total concentration of divalent ions was same in all experiments, but the Sr/Ca ratio was varied between 0.002 and 0.86, and the pH value was between 12.02 and 12.25. All solutions were oversaturated with respect to calcite (saturation index $\text{SI}_{\text{calcite}} = 1.2\text{--}1.5$). Calcite was the only product formed at low Sr/Ca ratios, but at $\text{Sr}/\text{Ca} \geq 0.45$ strontianite was detected in some systems. Sr-rich precipitate was observed in both a surface layer on rhombic calcite seed crystals ($6.9\text{--}6\ \mu\text{m}$) and as smaller calcite crystals ($>3.64\text{--}1.96\ \mu\text{m}$) that were elongated along their C-axis. The degree of crystal elongation increased with the Sr/Ca ratio in those crystals. Precipitates recovered from low Sr/Ca ratio experiments exhibited an XRD spectrum identical to that of rhombic calcite; however, the peaks attributed to Sr-containing calcite shifted progressively to lower 2θ values with increasing solution Sr/Ca ratio, indicating increased lattice volume. Sr K-edge EXAFS analysis of the precipitates showed that the shift in morphology and lattice volume is accompanied by a change in the local coordination of Sr^{2+} in calcite. The Sr–O bond lengths were similar to the Ca–O bond lengths in calcite, but Sr–O coordination increased from 6-fold in crystals containing 0.21 wt% Sr, to 8-fold in crystals containing 9.47 wt% Sr, and the Sr–Ca coordination decreased from 6 and 6 (for the first and second Sr–Ca shells, respectively) to 4 and 1. It is suggested that Sr^{2+} undergoes preferential incorporation at obtuse (+) growth sites on the calcite surface due to its large ionic radius (1.13 Å), and this increases the growth rate parallel to the C-axis, resulting in the observed elongation in this direction.



INTRODUCTION

The transfer of trace elements from solution to solid calcium carbonate has received a significant amount of interest across a range of fields. Measurements of the Sr content of biogenic carbonates, both aragonite and calcite, have been used to reconstruct paleo-climatic conditions.^{1–4} Trace element incorporation has been used to understand crystal growth.^{5–7} Furthermore, the co-precipitation of Sr into calcium carbonates has been proposed as an attenuation and remediation mechanism for ⁹⁰Sr contamination in groundwater.^{8–10}

The three main polymorphs of calcium carbonate found in geological deposits are calcite, aragonite, and vaterite, in order of decreasing stability. Calcite is characterized by rhombohedral coordination, with the central calcium atom surrounded by six oxygen atoms with Ca–O bond lengths of 2.36 Å; this is the most stable polymorph in most environmental settings. Aragonite has a more open structure. The central calcium atom is surrounded by nine oxygen atoms with Ca–O bond lengths of 2.42–2.66 Å.¹¹ Vaterite is the least stable calcium carbonate morphology, with the central calcium atom surrounded by eight oxygen atoms with Ca–O bond lengths

of 2.29–2.90 Å.¹¹ Aragonite formation is favored by high-temperature/high-pressure environments,¹² and by the presence of Mg^{2+} and SO_4^{2-} ions.^{6,13} Sulfate ions compete for the carbonate site, and, due to the larger sites in aragonite, sulfate hinders the growth of this polymorph the least.¹⁴ Magnesium ions compete for the calcium sites. Mg^{2+} ions are smaller than Ca^{2+} ions and, therefore, preferentially adsorb to calcite over aragonite, due to the smaller calcium sites therein. However, due to its higher hydration energy,¹⁵ Mg^{2+} retards growth at the calcite surface after adsorption, favoring the precipitation of aragonite. Furthermore, due to the presence of acute and obtuse growth sites at the calcite surface (which affects the geometry/size/adsorption properties of the calcite sites), Mg^{2+} affects the morphology of the calcite crystals by preferentially adsorbing to the acute sites due to its small ionic radius.⁶

The incorporation of Sr^{2+} into carbonates is dependent on a number of factors. Strontium may substitute for calcium in the

Received: November 21, 2017

Revised: April 10, 2018

Published: April 11, 2018

carbonate lattice due to similarities in their ionic radius and charge. However, strontium's larger ionic radius ($\text{Ca} = 1.0 \text{ \AA}$, $\text{Sr} = 1.13 \text{ \AA}$) introduces strain to the mineral lattice, eventually destabilizing it at high incorporation rates.^{16,17}

It has been proposed that, while incorporation of low levels of Sr^{2+} into the calcite lattice may be favorable (although the effect may be within error), increasing Sr^{2+} concentrations result in a sharp decrease in step growth speed at both obtuse and acute sites.¹⁸ This latter trend has been modeled by calculating step growth rates from a solid solution between rhombohedral calcite and strontianite end members, and by assuming that Sr^{2+} in the calcite lattice alters the ion activity product of CaCO_3 , resulting in a higher detachment rate of Ca^{2+} ions from the lattice, which slows step growth.¹⁶

Fast crystallization rates favor Sr^{2+} incorporation into calcite by minimizing the amount of time the Sr^{2+} is exposed at the calcite surface and able to be desorbed and replaced by a more favorable cation.^{18–21} Mg^{2+} is also known to enhance the incorporation of Sr^{2+} into calcite. Mg^{2+} is smaller than Ca^{2+} , which in conjunction with the larger Sr^{2+} ion balances the lattice strain, enabling greater Sr^{2+} incorporation.²² Strontium's local coordination environment within the carbonate lattice will also have a significant impact on its distribution coefficient. The larger M^{2+} sites in aragonite allow for greater incorporation of Sr^{2+} relative to calcite.²³ In previous work, Matsunuma et al.²⁴ used an amorphous calcium carbonate (ACC) pathway to improve the incorporation of trace metals such as Sr into the calcite lattice. Littlewood et al.²² found that this technique produced calcite through a vaterite intermediary, and that Sr^{2+} co-precipitated through this pathway retained its vaterite-like local environment (within the calcite crystals), indicating reaction pathways are critical for Sr incorporation into calcite.

This paper investigates how Sr is incorporated in calcite, and whether the mechanism of strontium incorporation into calcite changes as the amount of Sr incorporation increases. A series of constant solution composition experiments were conducted in a continuous tank stirred reactor that was seeded with calcite crystals. The total concentration of divalent ions in the reactor feedstock was constant across the experimental series, but the Sr/Ca ratio in individual experiments was varied between 0.002 and 0.86. Precipitates recovered from the reactor at different Sr/Ca ratios were analyzed by (i) scanning electron microscopy to observe the crystal morphology and determine the Sr/Ca ratio in different polymorphs by energy-dispersive spectroscopy, (ii) X-ray diffraction spectroscopy to determine minerals present and to provide information on their unit cell dimensions, (iii) and X-ray absorption spectroscopy to determine of the coordination environment around Sr ions incorporated into newly formed minerals.

EXPERIMENTAL SECTION

Continuous Tank Stirred Reactor (CTSR) Experiments. The CTSR consisted of a 150 mL spherical reaction vessel with two inlets for the mixed $\text{Ca}(\text{OH})_2/\text{SrCl}_2$ solution and Na_2CO_3 solution (Quickfit jointed borosilicate glassware). The divalent cations in the stock solution were maintained at a constant concentration of $8.73 \pm 0.34 \text{ mM}$, but the Sr/Ca ratio was varied. Na_2CO_3 was added at a nominal concentration of $50 \pm 0.024 \text{ mM}$ to all experiments. The divalent metal and carbonate solutions were fed into the reactor at constant rates of 135 mL h^{-1} (1.18 mmol h^{-1}) and 15 mL h^{-1} (0.75 mmol h^{-1}), respectively, to produce a constant solution composition within the reactor with an excess of M^{2+} ions. The pH of the reactor varied between 12.02 and 12.25. The output fluxes of M^{2+} ions was measured (see below), and the precipitation rate was calculated from the

difference between the input and output fluxes (it varied from 0.74 to 1.10 mmol h^{-1}).

Initial unseeded experiments produced both calcite and aragonite across a range of Sr:Ca ratios, with no systematic trend (see SI Table 1). Therefore, calcite seed crystals with a total mass of 0.73 g ($1 \text{ m}^2 \text{ L}^{-1}$) were added to the reactor at the start of the tests to ensure that calcite was the only polymorph produced (SI Table 2). The CTSR was initially run for 5 h (with a flow rate of 150 mL h^{-1} to replace 1 reactor volume/hour), after which time three solution samples ($\sim 4 \text{ mL}$) were taken at 1 h intervals to confirm that the solution composition in the reactor had equilibrated, and to determine the Ca:Sr ratio. Solution samples were filtered ($0.2 \mu\text{m}$ polyethersulfone hydrophilic filters), and the temperature and pH were determined using an Orion 420 pH meter with a VWR SJ113 probe (calibrated at pH 7.0, 10.01, and 12.46). A 1 mL subsample of the filtrate was then added to 9 mL of 0.1 M Aristar-grade HNO_3 (VWR International, USA) for chemical analysis.

At the end of each 7 h experiment, all the precipitate in the reactor was collected by passing the reactor solution through a Buchner filter with Sartorius Stedim Polycarbonate Track-Etch Membrane filter paper. The precipitate was thoroughly rinsed with isopropyl alcohol, after which it was stored in a desiccator. Subsamples of the precipitate ($\sim 4 \text{ mg}$) were dissolved in 10 mL of 0.1 M Aristar-grade HNO_3 for chemical analysis. Sr and Ca concentrations in the reactor solutions and the precipitate were determined by inductively coupled plasma optical emission spectroscopy (ICP-OES) (Thermo iCAP 7400, Thermo Fisher Scientific, Inc., USA).

Scanning Electron Microscopy (SEM) and Energy-Dispersive Spectroscopy (EDS). Precipitate samples were mounted on carbon tape, attached to aluminum stubs, and coated with iridium for SEM analysis on a FEI Quanta 650 Field Emission Gun SEM to investigate crystal morphology. One sample containing 6.36 wt% Sr was set in epoxy resin and polished using silicon carbide paper followed by a water-free diamond paste to provide a smooth surface for EDS analysis, which was carried out on a Tescan VEGA3 XM instrument, equipped with an X-max 150 SDD EDS and Aztec 3.3 data acquisition software.

X-ray Diffraction (XRD). Calcite precipitates recovered from the reactor at the end point of the experiments were mixed with a small portion of silicon standard and mounted on low-background silicon sample holders (the use of a standard enables the resultant XRD pattern to be corrected). Mineralogical analysis was carried out using a Bruker D8 XRD with a $\text{Cu K}\alpha_1$ source.

X-ray Absorption Spectroscopy (XAS). Sr K-edge (16105 eV) X-ray absorption spectra were collected from selected Sr-containing carbonate precipitates on beamline B18 at the Diamond Light Source. Samples were prepared as pressed pellets, dispersed with cellulose, and held in Kapton tape. Samples were mounted on a liquid nitrogen cryostat (80 K) during data collection to reduce the thermal disorder, improving the signal/noise ratio. At beamline B18, focusing of the beam produced for this experiment a spot size of approximately $1 \times 1 \text{ mm}^2$. Spectra were gathered from high-concentration samples in transmission mode, and in fluorescence mode (using a nine-element Ge solid state detector) for low-concentration samples. Multiple XAS scans from each sample were summed and averaged using Athena (version 0.9.25) to maximize the signal/noise ratio. Normalized X-ray absorption near-edge structure (XANES) data were plotted and compared to Sr K-edge XANES spectra collected from (Sr-containing) calcite,²⁵ aragonite,²⁶ and strontianite²⁷ standards. EXAFS spectra were then extracted and fitted in k -space using Artemis (version 0.9.25)²⁸ (k range = 3–13, r range = 1.1–4.3) to fit the data using the Markgraf and Reeder²⁵ calcite model structure.

RESULTS

XRD. XRD analysis of precipitate from the CTSR reactor experiment with a solution Sr/Ca ratio of 0.002 exhibited a peak profile consistent with calcite, displaying a maximum intensity peak at $29.4^\circ 2\theta$, and secondary peaks at 39.5° , 39.4° , 43.1° , 47.5° , and $48.5^\circ 2\theta$. These peaks are consistent with a

pure calcite sample. XRD analysis of the other precipitates from the CTSR reactor experiment exhibited essentially the same peak profile; however, the spectra showed clear variation with increasing wt% Sr (Figure 1). As the Sr content of the calcite

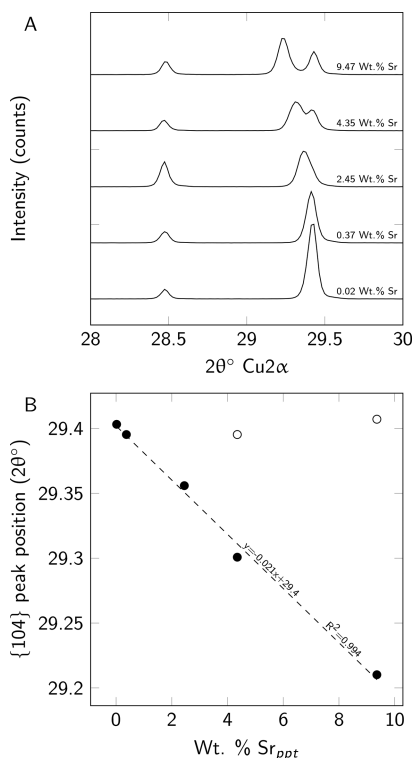


Figure 1. (A) XRD traces displaying peak broadening and subsequent splitting of the calcite {104} peak at $2\theta \approx 29.4^\circ$ (together with the silicon standard peak at $2\theta = 28.46^\circ$). (B) $2\theta^\circ$ position of the strained and unstrained {104} calcite peak (open and closed symbols, respectively).

increased, the peaks in the XRD spectra exhibited broadening and a shift in the maximum intensity to lower 2θ . Above 2.45 wt%, splitting of the calcite peaks was also observed. It is possible that this splitting was present in lower concentration samples but was masked by the proximity of the peaks (a clear asymmetry can be seen in the 2.45 wt% samples).

After Sr in the precipitate exceeded 9.23 wt%, strontianite was first detected in XRD patterns and became the dominant end product observed when Sr in the precipitate exceeded 9.36 wt% (SI Table 2). Precipitates containing detectable strontianite were not included in the subsequent analysis of Sr incorporation in calcite.

Sr/Ca Ratio in the Precipitates. In experiments where the precipitate contained less than 9.36 wt% Sr, there was an approximately linear relationship ($\text{Sr}/\text{Ca}_{\text{ppt}} = 0.15 \times \text{Sr}/\text{Ca}_{\text{aq}}$) between the Sr/Ca ratio measured in the precipitate and that measured in reactor solution (Figure 2). The gradient is equivalent to the Berthelot–Nernst distribution coefficient (eq 1). Three experiments where the saturation index, $\text{SI}_{\text{Strontianite}}$ was ≥ 2.2 produced precipitates with a $D_{\text{Sr}} > 0.2$.

$$D_{\text{Sr}} = \frac{[\text{Sr}]/[\text{Ca}]_{\text{ppt}}}{[\text{Sr}]/[\text{Ca}]_{\text{sol}}} \quad (1)$$

Precipitate Morphology. Precipitates from these experiments were characterized as a mixture of larger rhombs (mean

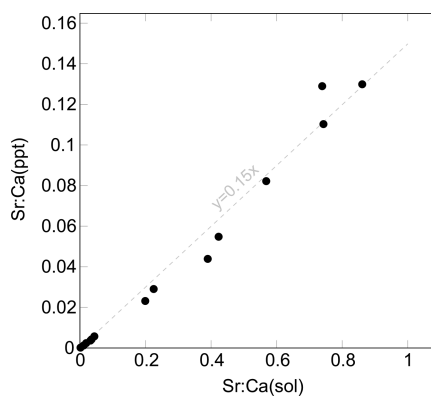
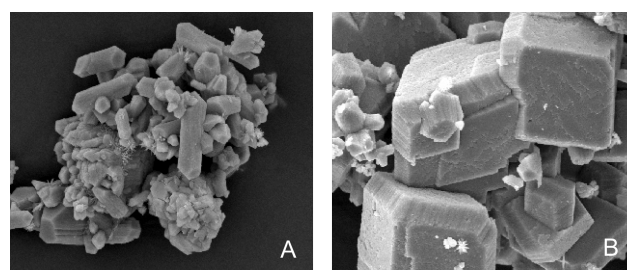


Figure 2. Variation in the Sr:Ca ratio in precipitates as a function of Sr:Ca ratio in solution. Trend line calculated by linear regression indicates $D_{\text{Sr}} = 0.15$.

6.9–6.0 μm) and smaller elongated crystals (mean 3.64–1.96 μm) with rhombic ends and cylindrical centers (Figure 3). With



5 μm

Figure 3. Two SEM images from an experiment with 9.36 wt% Sr displaying the two calcite morphologies: (A) elongated calcite and (B) rhombic calcite.

increasing wt% Sr, the elongated crystals present in the precipitate displayed a clear trend of increasing length/width ratio, summarized in Table 1. The larger rhombs had average length/width ratios of 0.87.

EDS. EDS mapping was carried out on four separate regions on a resin-embedded calcite sample with 6.36 wt% Sr. A representative back-scattered electron image (BSEI) and Sr, Ca, and O maps are included in Figure 4. The BSEI identifies a large rhombic crystal (lower right corner) and the fine elongated crystals (occupying the rest of the image). The Ca and O maps also highlight these crystals and indicate the crystals have uniform distribution of calcium and carbonate. The Sr map indicates that the rhombic crystals have Sr-rich rims but low Sr interiors, while Sr is more uniformly distributed in the elongated crystallites (SI Figure 3).

XAS. Analysis of strontium's coordination environment by XAS is presented in Table 2. The lowest wt% sample displays Sr–O, Sr–C, and Sr–Ca bond lengths and coordination values similar to those observed for Ca–O, Ca–C, and Ca–Ca in pure calcite. The lowest wt% sample displayed a peak at $\sim 16\,108$ eV and another at $\sim 16\,119$ eV (Figure 5). As the wt% Sr in the calcite increased, the 16 119 eV peak decreased in relative magnitude to become a shoulder to the 16 108 eV peak in the 9.47 wt% sample. This is consistent with a transition from a calcite-like coordination environment to a more strontianite/aragonite-like coordination environment (both

Table 1. Strontium Content and Distribution Coefficient, D_{Sr} , for the Range of Precipitates Analyzed

sample number	Sr/Ca		wt% Sr (solids)	D_{Sr} (solids)	L/W ^a (median)
	solution	precipitate			
50	0.00	0.00	0.02	0.10	1.59
65	0.01	0.00	0.11	0.11	
66	0.02	0.00	0.21	0.13	
58	0.03	0.00	0.32	0.11	
57	0.04	0.00	0.37	0.12	1.61
51	0.04	0.01	0.50	0.13	
59	0.20	0.02	1.96	0.12	
52	0.22	0.03	2.45	0.13	1.82
60	0.39	0.04	3.59	0.11	
53	0.42	0.05	4.35	0.13	2.13
61	0.57	0.08	6.36	0.14	
67	0.74	0.11	8.30	0.15	
54	0.86	0.13	9.36	0.15	2.50
63	0.74	0.13	9.47	0.17	

^aLength/width ratio, elongated crystals only; average of >100 measurements for each sample.

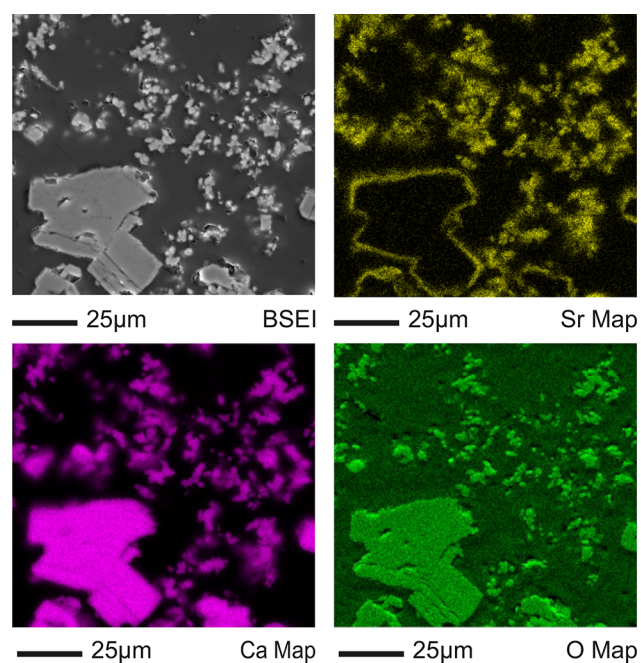


Figure 4. Back-scattered electron image (top left) with Sr, Ca, and O EDS element maps from a 6.36 wt% sample.

strontianite and aragonite have a 9-fold coordination environment around the divalent metal ion).

Fitting of EXAFS data suggests that low concentrations of Sr^{2+} (0.21 wt%) are able to fit into the calcite structure maintaining 6-fold Sr–O coordination, but with a Sr–O bond length of $2.43 \pm 0.09 \text{ \AA}$ (the Ca–O bond length in pure calcite is 2.36 \AA , from ref 22). At higher Sr incorporation (>1.96 wt%) the Sr–O bond length was similar ($2.44 \pm 0.02 \text{ \AA}$), but the best fit for Sr–O coordination increased to 7. The most concentrated sample (9.56 wt%) was best fit with 8-fold Sr–O coordination, more similar to that of strontianite/aragonite, although the Sr–O bond length is shorter than in strontianite (which has a Sr–O bond length of 2.59 \AA , from ref 27). Thus,

the Sr–O coordination number progressively increased with increasing Sr incorporation.

Coordination of Sr–C remained at 6 in all samples observed, with bond distances decreasing from 3.22 ± 0.09 to $2.93 \pm 0.05 \text{ \AA}$ in the 9.47 wt% sample. These fits show increased Debye–Waller (σ^2) values, which result from carbon’s low atomic mass and weak electron scattering, and indicate a higher degree of uncertainty in these values.

Bond lengths between Sr and the first and second shells of Ca atoms remained similar across the series (first shell $4.02\text{--}4.03 \text{ \AA}$, second shell $4.99\text{--}5.04 \text{ \AA}$); however, there was a progressive decrease in the transform amplitudes observed above 3 \AA (Figure 6B). As a result, the best-fit coordination numbers systematically decreased through the series from 6 and 6 for the first and second shells, respectively, in the 0.21 wt% sample to 4 and 1 in the 9.47 wt% sample.

DISCUSSION

Effect of Solution Composition on Reaction Product.

In this study, Sr-bearing calcites were precipitated that contained up to 9.36 wt% Sr, which was the upper limit for Sr incorporation to calcite observed in these experiments. Two samples displayed a greater Sr wt% (SI Table 2); however, XRD analysis indicates one contained strontianite alongside calcite, and both displayed $D_{Sr} > 2$. A $D_{Sr} > 2$ was therefore used to identify any further experiments which may have been affected by strontianite precipitation. D_{Sr} for Sr incorporation into calcite showed little variation prior to the formation of strontianite ($D_{Sr} = 0.10\text{--}0.17$), indicating similar rates of carbonate precipitation in these experiments.¹⁸ A minor increase in D_{Sr} was observed toward the upper end of our experimental range, prior to the detection of strontianite through XRD. This may indicate the formation of some strontianite below limits of detection for this technique.

Mode of Sr Incorporation into Calcite. The $\{104\}$ main XRD peak of Sr-substituted calcite, which is nominally at $2\theta = 29.4^\circ$, exhibits a linear trend of decreasing $2\theta^\circ$ position with increasing Sr wt% (Figure 1). This indicates that there is a progressive expansion of the calcite lattice volume with increasing Sr^{2+} incorporation.²⁴ Samples with 4.35 and 9.36 wt% Sr display peak splitting: the right-hand peak is Sr-free calcite (probably the seed crystals), while the left-hand peak results from calcite that has become disordered due to the presence of Sr (present both as overgrowths on rhombic seed crystals and as elongated crystals). The 2.45 wt% sample does not display splitting on the $\{104\}$ peak; however, this peak displays a shift in its $2\theta^\circ$, fitting on a linear trend with the other samples. It is therefore likely that this peak is a composite of two peaks—a pure calcite peak and a disordered Sr-calcite peak—which were too close together to be resolved by the XRD software. This interpretation is supported by the EXAFS data, which shows Sr is incorporated into the Ca site within the calcite lattice, and bond lengths calculated in Artemis suggest the strain imparted by increasing the Sr wt% causes a change in the coordination environment of Sr. An increase in the coordination of O-atoms around the Sr reflects a larger M^{2+} site. A decrease in the long-range Sr–Ca coordination was also observed, which indicates an expansion of the M^{2+} sites, resulting in increasing distortion of the calcite lattice. The local environment for Sr within calcite progressed from a rhombohedral calcite-like coordination to one more similar to the orthorhombic aragonite/strontianite structure (Figure 5). This coordination environment differs from that reported by

Table 2. EXAFS Fitting Parameters Calculated for Selected Calcite Samples in Artemis^a

	shell	N	R (Å)	σ^2	R-factor	χ^2
calcite ²⁵	O	6	2.36			
	C	6	3.21			
	Ca	6	4.05			
	Ca	6	4.99			
0.21 wt% Sr	O	6	2.43(9)	0.0043	0.034	1096
	C	6	3.19(7)	0.0176		
	Ca	6	4.03(1)	0.0061		
	Ca	6	4.94(2)	0.0066		
1.96 wt% Sr	O	7	2.44(1)	0.0050	0.023	782.43
	C	6	3.16(5)	0.0258		
	Ca	5	4.03(1)	0.0055		
	Ca	5	4.97(2)	0.0083		
3.59 wt% Sr	O	7	2.45(1)	0.0068	0.021	293.47
	C	6	2.78(6)	0.0266		
	Ca	4	4.05(1)	0.0067		
	Ca	3	5.02(3)	0.0085		
9.47 wt% Sr	O	8	2.45(1)	0.0066	0.01	1195.9
	C	6	2.93(5)	0.1243		
	Ca	4	4.03(1)	0.0083		
	Ca	1	5.04(4)	0.0043		
Sr-calcite ²² (6.4 wt%)	O	9	2.57			
	C	5	3.10			
	Ca	4	4.12			
aragonite ²⁶	O	9	2.58			
	C	6	2.98			
	Ca	6	4.02			
strontianite ²⁷	O	9	2.59			
	C	6	3.03			
	Sr	6	4.09			

^aLiterature data for calcite, aragonite, and strontianite are included for comparison.

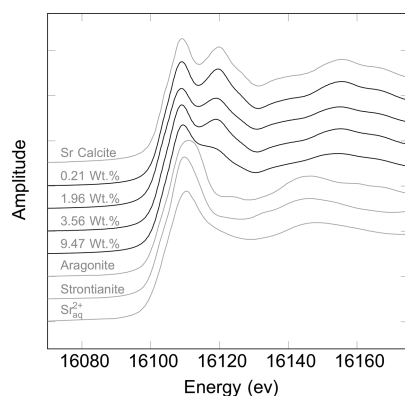


Figure 5. Sr XANES spectra collected from a series of increasing Sr wt % samples (black lines), plotted with selected standard data (gray).

Littlewood et al.,²² who found that when calcite was formed from the reordering of an ACC precursor through a vaterite intermediary, the Sr²⁺ was retained in a vaterite-like environment. The difference in Sr²⁺ coordination between this study and that reported by Littlewood et al.²² indicates that the

crystallization pathway impacts not only how effectively a trace element may be incorporated but also its local coordination environment.

Effect of Sr²⁺ on Calcite Morphology. SEM analysis of five precipitates ranging from 0.02 to 9.36 wt% Sr identified two distinct calcite morphologies, a rhombohedral form and an elongated form. Image analysis from these precipitates indicates that the L/W ratio of the elongated morphology displayed a systematic increase as the proportion of Sr in the precipitate increased (Table 1). This correlation between the L/W ratio and the Sr wt% implies that the incorporation of Sr favors the growth of a more elongated morphology.

EDS spot analysis indicates that the rhombohedral crystals contain very little Sr throughout their centers, although there is a Sr-rich layer at their surface. The Sr-poor core of the rhombic crystals is similar in size to the added calcite seed crystals (SI Figure 4); therefore, the rhombic crystal very likely represents a retained fraction of the seed crystals that have been overgrown with Sr-rich calcite during the experiments. Indeed, XRD patterns show peaks from two separate calcite phases, one identical to pure Sr-free calcite and the other strained by Sr incorporation, with no evidence for multiple Sr-containing

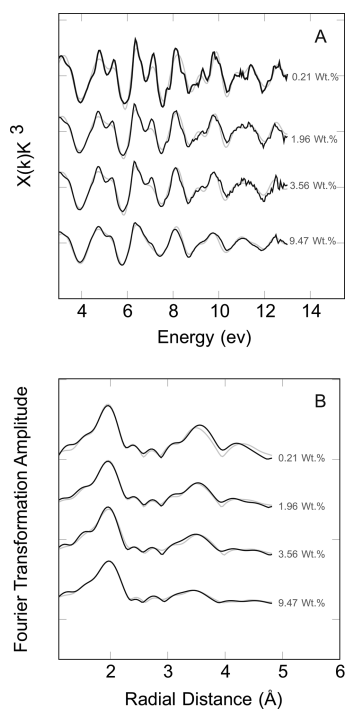


Figure 6. (A) EXAFS spectra collected from a series of increasing Sr wt% samples and (B) corresponding Fourier transformations (FT). Model fits using the data shown in Table 2 are also provided for each sample in gray.

phases. EDS indicates that the maximum concentration of Sr in the Sr-rich overgrowths on rhombic crystals is similar to the average concentration of the smaller elongated crystals. However, Sr incorporation in the overgrowth layer was typically lower than in the elongated crystals, potentially due to the averaging effects of the EDS spot and the narrow rim of Sr incorporation displayed by the rhombic crystals. Therefore, we conclude that both the overgrowths and the elongated crystals may have similar amounts of Sr incorporation (although the mechanism of incorporation may be different).

The SEM-EDS, XRD, and EXAFS data together show that Sr is incorporated into calcite and is primarily hosted within its lattice rather than present in surface sorption complexes. It is also clear that greater incorporation of Sr leads to a change in the local coordination environment of the Sr ion and a greater observed elongation of the initially smaller particles.

Several studies have identified a similar elongated calcite morphology displaying elongation about the *c*-axis produced by the presence of Mg^{2+} and organic compounds.^{6,29,30} Atomic force microscopy maps published by Davis et al.⁶ suggest that Mg^{2+} affects the propagation of calcite growth steps by preferentially adsorbing to the acute step sites, causing retardation of the growth rate for these sites and leading to anisotropy in kink propagation.

Due to its larger ionic radius relative to calcium, it is expected that Sr^{2+} will preferentially adsorb to the obtuse sites rather than the acute sites. The enhanced growth rate parallel to the *c*-glide plane suggests that this incorporation of Sr^{2+} is enhancing the growth rate of the obtuse face (Figure 7),³¹ suggesting that low concentrations of Sr^{2+} may enhance the calcite growth rate as it is contributing to the net precipitation rate. Step growth rate data³² (which are supported by modeling³¹) display a more rapid step speed for obtuse steps, with the difference between obtuse and acute steps becoming greater with increasing SI. It is

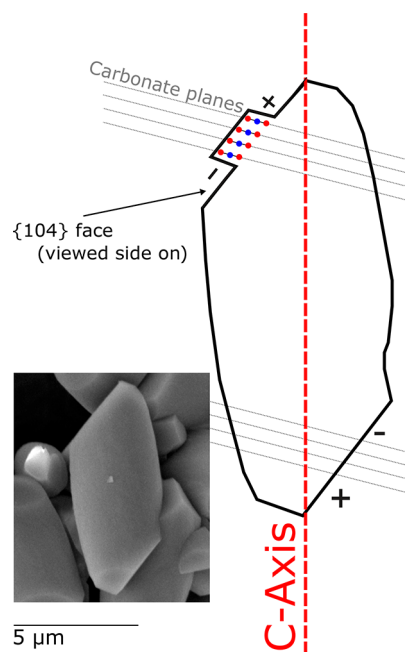


Figure 7. Schematic image based on a crystal from the 2.45 wt% system, displaying a side-on view of the {104} face and elongating parallel to the *c*-axis. A schematic image of the inclination of the carbonate planes with respect to the {104} face is included based on ref 32.

likely that our experiments, which were carried out at SI = 1.2–1.5 rather than the SI = 0.24–0.51 used to measure the step growth rates, would display an even greater obtuse step speed relative to acute steps. Additionally, a threshold followed by a rapid decline in the step growth rates with increasing $[Sr^{2+}]$ is reported.³² This threshold results from the impact of trace ions on the solubility of calcite. As the proportion of strontium ions within the lattice increases, the lattice bonds become less stable and the rate of ion detachment increases; this effectively destabilizes the formation of calcite.¹⁶ This threshold is encountered at increasing $[Sr^{2+}]$ with increasing SI, and since our experiments were carried out at greater SI than those presented in ref 32, it is likely that the threshold was not encountered during our experiments.

Sr^{2+} incorporation into calcite produces an elongated crystal similar to that observed by Mg^{2+} incorporation⁶ but does so by different mechanisms. Sr^{2+} adsorbs to obtuse sites and enhances growth parallel to the *c*-glide plane, whereas Mg^{2+} adsorbs to acute sites due to its relatively small ionic radius and retards growth due to its relatively high hydration energy,¹⁵ thus restricting growth orthogonal to the *c*-glide plane. We suggest that the rhombic morphology does not show similar elongation to the elongated morphology due to the nature of the Sr incorporation; i.e., it is a thin surface layer which cannot influence the shape of the bulk crystal.

CONCLUSIONS

A suite of calcite precipitates displaying a range of Sr^{2+} concentrations were produced in a constant composition reactor. These calcites exhibited increased lattice volume associated with increased Sr content. At low concentrations the Sr^{2+} ion displayed a local environment similar to that of Ca in calcite; with higher concentrations this became more aragonite/strontianite-like yet retained a short Sr–O bond

length. The presence of Sr²⁺ during calcite growth was found to affect the morphology of the resultant calcite. Precipitates containing greater Sr contents displayed an elongation about their *c*-axis, most likely caused by preferential adsorption of Sr²⁺ at the obtuse growth steps, allowing an enhanced growth rate at these sites. This study shows that Sr-containing calcite can be produced at relatively high D_{Sr} values in high-throughput reactors across a broad range of Sr concentrations. Therefore, controlled Sr-calcite precipitation may potentially be used to remove ⁹⁰Sr from waste waters present at nuclear sites.

■ ASSOCIATED CONTENT

📄 Supporting Information

The Supporting Information is available free of charge on the ACS Publications website at DOI: 10.1021/acs.cgd.7b01614.

Additional XRD data, SEM images, EDS data, and a data table comprising more detailed information about the experimental conditions (PDF)

■ AUTHOR INFORMATION

Corresponding Author

*E-mail: i.t.burke@see.leeds.ac.uk. Phone: +44 113 3437532. Fax: +44 113 3435259.

ORCID

David J. Hodkin: 0000-0003-1265-6472

Douglas I. Stewart: 0000-0001-5144-1234

Ian T. Burke: 0000-0002-0484-568X

Notes

The authors declare no competing financial interest.

■ ACKNOWLEDGMENTS

We thank Andy Connelly, Stephen Reid, Lesley Neve, and Duncan Hedges from the University of Leeds for help with BET, ICP-OES, XRD, ICP-OES, and SEM analysis, respectively. The research was funded by a UK Nuclear Decommissioning Authority Ph.D. bursary to D.J.H. and beamtime awards at Beamline B18 at the Diamond Light source, UK.

■ REFERENCES

- (1) Weber, J. N. Incorporation of Strontium into Reef Coral Skeletal Carbonates. *Geochim. Cosmochim. Acta* **1973**, *37*, 2173–2190.
- (2) de Villiers, S.; Shen, G. T.; Nelson, B. K. The Sr/Ca-Temperature Relationship in Coralline Aragonite: Influence of Variability in (Sr/Ca)Seawater and Skeletal Growth Parameters. *Geochim. Cosmochim. Acta* **1994**, *58*, 197–208.
- (3) Stoll, H. M.; Klaas, C. M.; Probert, I.; Encinar, J. R.; Garcia Alonso, J. I. Calcification Rate and Temperature Effects on Sr Partitioning in Coccoliths of Multiple Species of Coccolithophorids in Culture. *Glob. Planet. Change* **2002**, *34*, 153–171.
- (4) Ruiz-Hernandez, S. E.; Grau-Crespo, R.; Ruiz-Salvador, A. R.; De Leeuw, N. H. Thermochimistry of Strontium Incorporation in Aragonite from Atomistic Simulations. *Geochim. Cosmochim. Acta* **2010**, *74*, 1320–1328.
- (5) De Yoreo, J. J.; Dove, P. M. Shaping Crystals with Biomolecules. *Science* **2004**, *306*, 1301–1302.
- (6) Davis, K. J.; Dove, P. M.; Wasylenko, L. E.; De Yoreo, J. J. Morphological Consequences of Differential Mg²⁺ Incorporation at Structurally Distinct Steps on Calcite. *Am. Mineral.* **2004**, *89*, 714–720.
- (7) Paquette, J.; Reeder, R. J. Relationship between Surface Structure, Growth Mechanism, and Trace Element Incorporation in Calcite. *Geochim. Cosmochim. Acta* **1995**, *59*, 735–749.

- (8) Fujita, Y.; Ferris, F. G.; Lawson, R. D.; Colwell, F. S.; Smith, R. W. Calcium Carbonate Precipitation by Ureolytic Subsurface Bacteria. *Geomicrobiol. J.* **2000**, *17*, 305–318.

- (9) Warren, L. A.; Maurice, P. A.; Parmar, N.; Ferris, G. F. Microbially Mediated Calcium Carbonate Precipitation: Implications for Interpreting Calcite Precipitation and for Solid-Phase Capture of Inorganic Contaminants. *Geomicrobiol. J.* **2001**, *18*, 93–115.

- (10) Mitchell, A. C.; Ferris, F. G. The Coprecipitation of Sr into Calcite Precipitates Induced by Bacterial Ureolysis in Artificial Groundwater: Temperature and Kinetic Dependence. *Geochim. Cosmochim. Acta* **2005**, *69*, 4199–4210.

- (11) Blanco-Gutierrez, V.; Demourgues, A.; Jubera, V.; Gaudon, M. Eu(III)/Eu(II)-Doped (Ca 0.7 Sr 0.3) CO₃ Phosphors with Vaterite/calcite/aragonite Forms as Shock/temperature Detectors. *J. Mater. Chem. C* **2014**, *2*, 9969–9977.

- (12) Burton, E. A.; Walter, L. M. Relative Precipitation Rates of Aragonite and Mg Calcite from Seawater: Temperature or Carbonate Ion Control? *Geology* **1987**, *15*, 111–114.

- (13) Bots, P.; Benning, L. G.; Rickaby, R. E. M.; Shaw, S. The Role of SO₄ in the Switch from Calcite to Aragonite Seas. *Geology* **2011**, *39*, 331–334.

- (14) Fernández-Díaz, L.; Fernández-González, Á.; Prieto, M. The Role of Sulfate Groups in Controlling CaCO₃ Polymorphism. *Geochim. Cosmochim. Acta* **2010**, *74*, 6064–6076.

- (15) Rodríguez-Cruz, S.; Jockusch, R.; Williams, E. R. Hydration Energies and Structures of Alkaline Earth Metal Ions, M²⁺ (H₂O)_N, N= 5–7, M= Mg, Ca, Sr, and Ba. *J. Am. Chem. Soc.* **1999**, *121*, 8898–8906.

- (16) Nielsen, L. C.; De Yoreo, J. J.; DePaolo, D. J. General Model for Calcite Growth Kinetics in the Presence of Impurity Ions. *Geochim. Cosmochim. Acta* **2013**, *115*, 100–114.

- (17) Tesoriero, A. J.; Pankow, J. F. Solid Solution Partitioning of Sr²⁺, Ba²⁺, and Cd²⁺ to Calcite. *Geochim. Cosmochim. Acta* **1996**, *60*, 1053–1063.

- (18) Lorens, R. B. Sr, Cd, Mn and Co Distribution Coefficients in Calcite as a Function of Calcite Precipitation Rate. *Geochim. Cosmochim. Acta* **1981**, *45*, 553–561.

- (19) Gabitov, R. I.; Watson, E. B. Partitioning of Strontium between Calcite and Fluid. *Geochim., Geophys., Geosyst.* **2006**, *7*, 1216.

- (20) Tang, J.; Köhler, S. J.; Dietzel, M. Sr²⁺/Ca²⁺ and 44Ca/40Ca Fractionation during Inorganic Calcite Formation: I. Sr Incorporation. *Geochim. Cosmochim. Acta* **2008**, *72* (15), 3718–3732.

- (21) Gabitov, R. I.; Sadekov, A.; Leinweber, A. Crystal Growth Rate Effect on Mg/Ca and Sr/Ca Partitioning between Calcite and Fluid: An in Situ Approach. *Chem. Geol.* **2014**, *367*, 70–82.

- (22) Littlewood, J. L.; Shaw, S.; Peacock, C. L.; Bots, P.; Trivedi, D.; Burke, I. T. Mechanism of Enhanced Strontium Uptake into Calcite via an Amorphous Calcium Carbonate Crystallization Pathway. *Cryst. Growth Des.* **2017**, *17*, 1214–1223.

- (23) Curti, E. Coprecipitation of Radionuclides with Calcite: Estimation of Partition Coefficients Based on a Review of Laboratory Investigations and Geochemical Data. *Appl. Geochem.* **1999**, *14*, 433–445.

- (24) Matsunuma, S.; Kagi, H.; Komatsu, K.; Maruyama, K.; Yoshino, T. Doping Incompatible Elements into Calcite through Amorphous Calcium Carbonate. *Cryst. Growth Des.* **2014**, *14*, 5344–5348.

- (25) Markgraf, S.; Reeder, R. High-Temperature Structure Refinements of Calcite and Magnesite. *Am. Mineral.* **1985**, *70*, 590–600.

- (26) Finch, A. a.; Allison, N. Coordination of Sr and Mg in Calcite and Aragonite. *Mineral. Mag.* **2007**, *71*, 539–552.

- (27) De Villiers, J. P. R. Crystal Structures of Aragonite, Strontianite, and Witherite. *Am. Mineral.* **1971**, *56*, 758–767.

- (28) Ravel, B.; Newville, M. ATHENA, ARTEMIS, HEPHAESTUS: Data Analysis for X-Ray Absorption Spectroscopy Using IFEFFIT. *J. Synchrotron Radiat.* **2005**, *12*, 537–541.

- (29) Ukrainczyk, M.; Greiner, M.; Elts, E.; Briesen, H. Simulating Preferential Sorption of Tartrate on Prismatic Calcite Surfaces. *CrystEngComm* **2015**, *17*, 149–159.

(30) Kim, I. W.; Collino, S.; Evans, J. S. Cooperative Modulation of Mineral Growth by Prismatic-Associated Asprich Sequences and Mg(II). *Int. J. Mol. Sci.* **2012**, *13*, 3949–3958.

(31) Nielsen, M. H.; Aloni, S.; De Yoreo, J. J. In Situ TEM Imaging of CaCO₃ Nucleation Reveals Coexistence of Direct and Indirect Pathways. *Science* **2014**, *345* (6201), 1158–1162.

(32) Wasylenki, L. E.; Dove, P. M.; Wilson, D. S.; De Yoreo, J. J. Nanoscale Effects of Strontium on Calcite Growth: An in Situ AFM Study in the Absence of Vital Effects. *Geochim. Cosmochim. Acta* **2005**, *69*, 3017–3027.